NANO LETTERS

Letter

pubs.acs.org/NanoLett

Real-Time Visualization of Nanocrystal Solid–Solid Transformation Pathways

Joshua S. Wittenberg,[†,‡] Timothy A. Miller,[‡] Erzsi Szilagyi,[§] Katie Lutker,[∥] Florian Quirin,[⊥] Wei Lu,[⊥] Henrik Lemke,[■] Diling Zhu,[■] Matthieu Chollet,[■] Joseph Robinson,[■] Haidan Wen,[●] Klaus Sokolowski-Tinten,[⊥] A. Paul Alivisatos,[∥] and Aaron M. Lindenberg*[,†,‡,▲]

[†]Department of Materials Science and Engineering, Stanford University, Stanford, California 94305, United States

[‡]Stanford Institute for Materials and Energy Sciences, SLAC National Accelerator Laboratory, 2575 Sand Hill Road, Menlo Park, California 94025, United States

[§]Department of Chemistry, Stanford University, Stanford, California 94305, United States

[∥]Department of Chemistry, University of California, Berkeley, Berkeley, California 94720, United States

[⊥]Faculty of Physics and Center for Nanointegration Duisburg-Essen (CENIDE), University of Duisburg-Essen, Lotharstrasse 1, 47048, Duisburg, Germany

[■]Linac Coherent Light Source, SLAC National Accelerator Laboratory, Menlo Park, California 94025, United States

[●]Advanced Photon Source, Argonne National Laboratory, Argonne, Illinois 60439, United States

[▲]Stanford PULSE Institute, SLAC National Accelerator Laboratory, Menlo Park, California 94025, United States

Supporting Information

ABSTRACT: Measurement and understanding of the microscopic pathways materials follow as they transform is crucial for the design and synthesis of new metastable phases of matter. Here we employ femtosecond single-shot X-ray diffraction techniques to measure the pathways underlying solid–solid phase transitions in cadmium sulfide nanorods, a model system for a general class of martensitic transformations. Using picosecond rise-time laser-generated shocks to trigger the transformation, we directly observe the transition state dynamics associated with the wurtzite-to-rocksalt structural phase transformation in cadmium sulfide with atomic-scale resolution. A stress-dependent transition path is observed. At high peak stresses, the majority of the sample is converted directly into the rocksalt phase with no evidence of an intermediate prior to rocksalt formation. At lower peak stresses, a transient five-coordinated intermediate structure is observed consistent with previous first principles modeling.

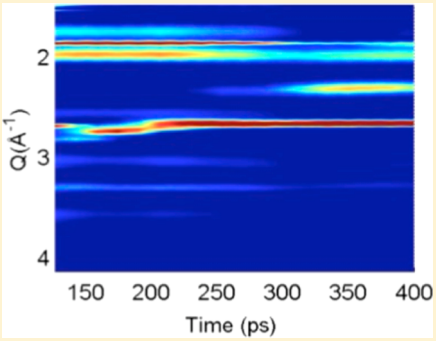

KEYWORDS: *Structural phase transition, martensitic, shock, time-resolved, X-ray*

Martensitic phase transitions are first-order diffusionless transformations involving short-range collective atomic motion with well-defined transition pathways between closely related crystal structures. They are central to many naturally occurring phenomena including compression during tectonic motion and the release of DNA from viral capsids into host cells[1,2] and have been utilized in technological applications ranging from the ancient practice of tempering steel to modern work on shape memory alloys.[2,3] One of the outstanding challenges in the study of this type of phase transition has been an understanding of the microscopic transformation pathways by which they are defined, with the first steps occurring on picosecond time-scales and atomic length-scales.[4−6] In the case of bulk materials, measurements are obscured by extensive uncorrelated nucleation events occurring throughout the sample, which impinge upon one another as they grow. In contrast, colloidally grown nanocrystals represent a model system with which to study phase transformations because they are defect-free single crystalline domains.[7−9] Nucleation is a rare event under hydrostatic compression near the transformation pressure, while the phase front across a single particle propagates at the sound speed of the material. As a result, a given particle will typically transform fully before another stable nucleus can form (a few picoseconds for a few-nanometer diameter particle), separating the competing events of nucleation of the new phase from its subsequent growth. An ensemble of small, independent domains therefore exhibits first-order transformation kinetics similar to many chemical reactions and is described by transition state theory with nucleation constituting the activation barrier.[10−12] Recent simulations of the pressure-induced wurtzite-to-rocksalt trans-

Received: January 6, 2014
Revised: February 21, 2014
Published: March 3, 2014

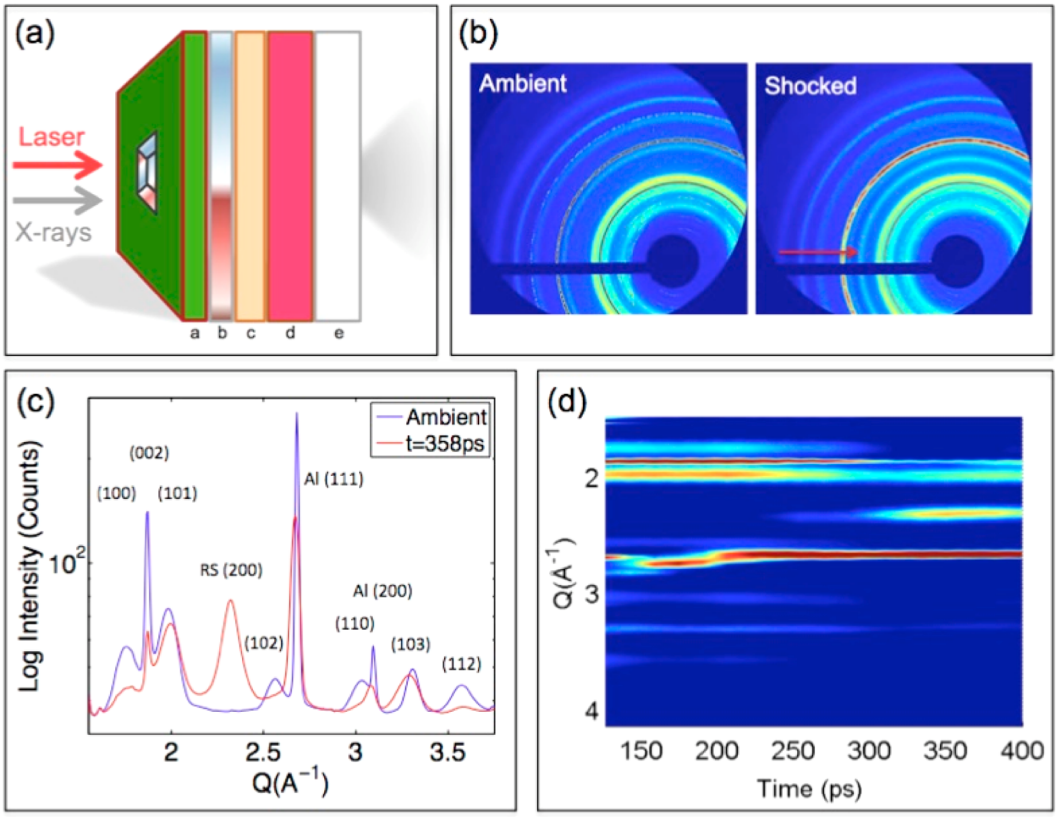

Figure 1. (a) Sample schematic consisting of a 2 μm thick Si_3N_4 window (a), vapor coated with 250 nm of aluminum (b), a 1 μm thick polyvinylalcohol (PVA) buffer layer (c), a 250 nm layer of CdS nanocrystals drop-cast from toluene solution (d), and a 2 μm thick PVA overlayer for inertial confinement (e). (b) Raw data showing X-ray scattering pattern from nanocrystals at ambient pressure (left) and at 300 ps following shock compression, (right) with the emerging rocksalt (200) reflection indicated. (c) Azimuthally integrated Q-dependent diffraction patterns before and after compression. (d) Scattered intensity as a function of momentum transfer Q (vertical axis) and pump−probe delay (horizontal axis) at ~9 GPa applied stress.

formation in semiconductor nanocrystals using transition path sampling and molecular dynamics methods have been able to suggest possible transition states for these processes.[13−17] In particular, a two-stage model consisting of compression along the *c*-axis to form a five-coordinate *h*-MgO type intermediate followed by compressive shear along the *a*-axis to the cubic rocksalt structure with the transformation rate limited by the shear step has been proposed. No experimental measurement of this proposed mechanism has been possible to date. Here, using laser-generated picosecond-rise-time high pressure shocks to trigger the transformation coupled with femtosecond X-ray pulses as a structural probe, we have obtained direct information about the transformation pathway associated with the wurtzite to rocksalt structural phase transition in cadmium sulfide (CdS) nanorods. Nanocrystals shocked to lower peak stresses are indeed preferentially compressed along the *c*-axis toward a five-coordinate *h*-MgO type intermediate structure, as predicted by simulations, whereas those shocked more strongly exhibit no evidence of an *h*-MgO type intermediate structure during the transformation to rocksalt. Additionally, we observe the wurtzite-to-rocksalt polymorphic phase transformation in CdS nanorods occurring on time-scales approximately 10 orders of magnitude faster than previously observed kinetic time-scales, in agreement with previous indirect observations of shear-catalyzed transitions.[18]

We made use of standard laser-based ablative techniques to generate large amplitude shocks.[19−21] Figure 1a shows the sample geometry with a ~250 nm layer of 40 nm × 5 nm CdS rods (randomly oriented) deposited on a Si_3N_4 substrate with a thin aluminum layer to generate the shocks and polyvinyl alcohol layers to both steepen the shock front and provide inertial confinement (Figure 1a).[22] Experiments were carried out at the Linac Coherent Light Source (LCLS) X-ray pump−probe (XPP) hutch using hard X-ray scattering in a collinear, transmission geometry using the undulator fundamental at 9.5 keV X-ray energy and 70 fs fwhm pulse duration and recorded on a large-area MAR detector shot-by-shot.[23,24] Optical pulses with a central wavelength of 800 nm, stretched to 1 ps fwhm pulse duration to minimize their nonlinear absorption in the Si_3N_4 substrate, were used to initiate shock waves with stresses between 2 and 10 GPa. These shock generation pulses were focused to 250 μm in order to ensure oversampling of the 50 μm diameter X-ray focal spot. Because each shocked region of the target was destroyed by a single laser pulse, the target array was translated after each shot in order to study a fresh sample of nanocrystals.

Figure 1b shows single X-ray pulse scattering images comparing the ambient pressure sample to the transiently compressed sample, in good agreement with the known diffractograms at ambient and high pressure, showing the emergence of the (200) rocksalt peak indicating the nanocrystal transformation has occurred. Azimuthally integrated lineouts and associated dynamics are depicted in Figure 1c,d. At short times, the aluminum (111) diffraction peak ($Q = 2.68$ Å^{-1}) ($Q = 4\pi \sin(\theta)/\lambda$ shifts to higher Q associated with a large amplitude compression. Figure 2a displays azimuthally

dx.doi.org/10.1021/nl500043c | *Nano Lett.* 2014, 14, 1995−1999

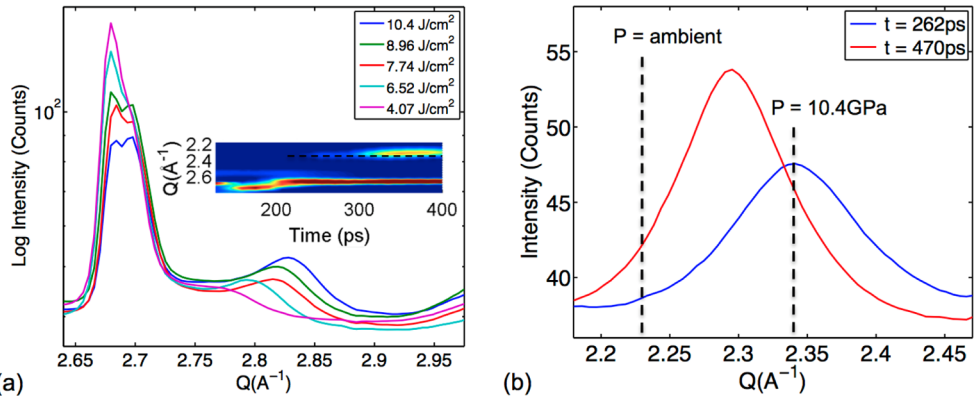

Figure 2. (a) Fluence dependence of aluminum (111) reflection at maximum compression. Inset: Zoom diffractogram of aluminum and rocksalt dynamics shown as a function of momentum transfer and time. (b) Q-dependence of shock-induced rocksalt reflection shown at t = 262 ps (blue) and at t = 470 ps (red) showing maximum deflection of peak and subsequent relaxation toward ambient pressure.

integrated lineouts of the aluminum peak as a function of incident laser fluence, showing both an induced shoulder on the main aluminum peak in addition to a well-separated sideband, which can be associated with uniaxial elastic and isotropic plastic compressions, respectively, with the plastic response dominating the observed diffraction peak shifts (see Supporting Information) and developing on ∼10 ps time scales. These results are consistent with earlier studies[25−29] and first principles MD simulations.[30] We estimate peak stresses of approximately 12 GPa generated within the aluminum layer (Supporting Information).

After a time-delay associated with the propagation of the shock through the target layers, the rocksalt (200) peak (Q = 2.3 Å^{-1}) appears (Figure 2b), and the wurtzite (100) intensity decreases (1.76 Å^{-1}), indicating the formation of rocksalt and the disappearance of wurtzite CdS, respectively. There is no significant change in the wurtzite (101) reflection (1.98 Å^{-1}), since the decrease in intensity is replaced with scattering from the rocksalt (111) reflection. The wurtzite reflections at higher scattering angle ((110), (103), (112)) also decrease in intensity and broaden; this region is more difficult to interpret because the induced rocksalt (220) reflection overlaps with these peaks.[11] We can obtain an approximate measure of the pressure within the nanocrystal layer directly by recording the rocksalt (200) scattering angle relative to the known ambient rocksalt (200) position, as shown in Figure 2b.[31] Combining the extracted strain with the known bulk modulus in the rocksalt phase yields the pressure directly, under the assumption of isotropic compression in the product phase, as would be expected for plastic deformation. This corresponds to maximum generated pressures of ∼10 GPa (Figure 2b), roughly consistent with the estimates obtained from the aluminum response.

The fraction of the sample that is converted to rocksalt is dependent upon the excitation fluence (Figure 3) with a threshold behavior observed. First evidence of the phase transition occurs at ∼5 GPa on approximately 50 ps time-scales, slightly less than the known kinetic transition pressure for nanocrystals.[11] The rocksalt phase persists for at least 8 ns (Supporting Information) consistent with previous studies indicating metastability.[32]

The actual microscopic mechanism of the wurtzite to rocksalt phase transformation has been the most elusive piece of information in previous experiments. A 4 nm spherical particle should transform in 7−10 ps, based on simulations.[13] The

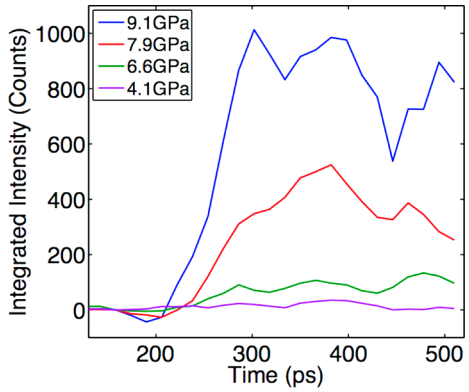

Figure 3. Rocksalt radially integrated intensity as a function of time and applied stress.

sample particles, at 40 nm × 5 nm are therefore expected to transform within 40−80 ps, depending on where in the particle the rocksalt nucleus forms. A shock front traveling at 5 nm/ps[33] through the dense composite traverses the 250 nm sample layer within ∼50 ps. Accounting for this transit time, the 70 ps rise time observed is consistent with the rapid rate of transformation observed in simulations. Two sets of diffractograms collected during this experiment are presented in Figure 4. The patterns are from samples shocked to (a) 4.1 and (c) 9.1 GPa. At low peak stress, following time zero there is a shift in the wurtzite (002) reflection to higher scattering angle, without a change in the wurtzite (100), the reflection with no component along the c-axis (Figure 4a). This indicates a preferential compression along the nanorod c-axis (long axis). Such a decrease in the c/a ratio is consistent with the predicted formation of the h-MgO intermediate pathway. Rietveld refinement (Supporting Information) indicates quantitative agreement between the experimentally determined c/a and this first principles modeling, including the existence of the predicted h-MgO phase. The wurtzite (101) exhibits a smaller shift, consistent with its smaller c-axis component. The (002) peak returns to lower Q at later times (Figure 4b), evidence that the structure produced is an unstable intermediate with a negligible activation barrier for returning to the pure wurtzite structure. This is consistent with simulations[13] that indicate that the h-MgO formation proceeds gradually as the pressure is ramped up, such that nucleation of the rocksalt phase is the rate limiting step. In contrast, at the highest stresses evidence for the

dx.doi.org/10.1021/nl500043c | Nano Lett. 2014, 14, 1995−1999

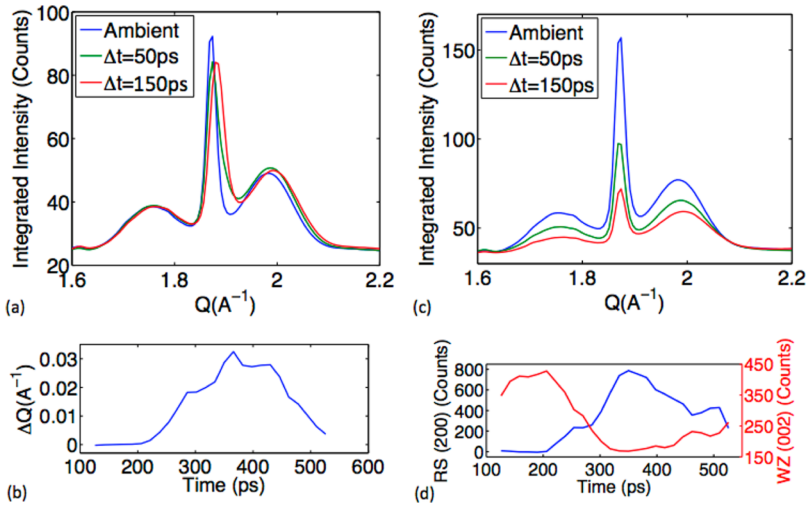

Figure 4. Evidence for production of *h*-MgO-type intermediate phase at low shock stresses. Evolution of wurtzite lineshapes as a function of the time following shock arrival at 4.1 (a) and 9.1 (c) GPa. (b) Time-dependent shift in wurtzite (002) reflection at 4.1 GPa. (d) Simultaneous increase in rocksalt (200) and decrease in wurtzite (002) at 9.1 GPa.

intermediate structure is not observed (Figure 4c), which shows a large amplitude reduction in the (002) reflection without measurable shift as the majority of the sample switches into the high pressure phase for which the (002) reflection is forbidden. Figure 4d shows that this reduction occurs concurrently with the rocksalt (200) increase.

One can extract further information from the fact that there is no clear evolution of the entire diffractogram from the intermediate structure to the rocksalt structure. The shock traverses approximately one-third of the sample layer in 16 ps, the time step for this experiment. Thus, given the above estimates of the single particle transformation time, a significant fraction of the particles in the sample layer should still be in the process of transformation, which is not observed. This indicates that an alternative pathway to rocksalt exists with no preceding intermediate. In contrast, at the lowest shock stresses applied there is indeed a shift of the wurtzite (002) reflection (Figure 4a). Such a change in transformation pathway under shock compression is consistent with the rapid transformation rate we have observed, as compared with experiments carried out under hydrostatic conditions, and indicates a reduction in the activation barrier for the transformation under shock compression.[11] This may be compared to recent simulations that have suggested that spherical nanoparticles with a more disordered surface do not pass through a five-coordinate intermediate structure on the way to rocksalt, whereas well-faceted particles do transform via such an intermediate.[14] We note that the homogeneous decrease in the (002) reflection (Figure 4c) without significant broadening as the rocksalt (200) appears is inconsistent with a large number of nucleation sites per nanocrystal and is more consistent with a coherent transformation of the entire rod at the highest pressures.[34] Indeed, a Debye−Scherrer estimate using the width of the induced (200) reflection yields domain sizes of order 10 nm, comparable to the size of the nanorod itself.

This work constitutes the first experimental measurement of a nanocrystal transformation pathway. Below the transformation threshold, the structure approaches the five-coordinate *h*-MgO type intermediate observed under simulated hydrostatic compression. When brought above the transformation threshold by shock compression, however, the *h*-MgO structure is not observed. The decreasing prevalence of the intermediate with increasing shock stress indicates that a different pathway for the transformation becomes possible at high shock stresses, in close analogy with the action of a catalyst in chemical reactions.

■ ASSOCIATED CONTENT

Ⓢ Supporting Information

Estimation of induced pressure jump, long time (nanosecond) data, Rietveld refinement, and TEM studies. This material is available free of charge via the Internet at http://pubs.acs.org.

■ AUTHOR INFORMATION

Corresponding Author

*E-mail: aaronl@stanford.edu.

Author Contributions

J.S.W., T.A.M., E.S., K.L., F.Q., H.L., D.Z., M.C., J.R., H.W., K.S.T., and A.M.L. carried out the experiment. W.L. performed supporting diffraction calculations. J.S.W., A.P.A., and A.M.L. initiated the project and conceived the work. J.S.W. and A.M.L. wrote the manuscript with input from all authors.

Notes

The authors declare no competing financial interest.

■ ACKNOWLEDGMENTS

This work was supported by the Department of Energy, Basic Energy Sciences, Materials Sciences and Engineering Division. Portions of this research were carried out at the Linac Coherent Light Source (LCLS) at the SLAC National Accelerator Laboratory. LCLS is an Office of Science User Facility operated for the U.S. Department of Energy (DOE) Office of Science by Stanford University. H.W. acknowledges support from U.S. Department of Energy, Office of Science, under Contrast No. DE-AC02-06CH11357. F.Q. and K.S.T. gratefully acknowledge financial support by the German Research Council through the Collaborative Research Center SFB 616 "Energy Dissipation at Surfaces". K.M.L. and A.P.A. are supported by the Physical Chemistry of Inorganic Nanostructures Program, KC3105, Director, Office of Science, Office of Basic Energy Sciences, of the United States Department of Energy under contract DE-AC02-05CH11231.

REFERENCES

(1) Mateu, M. G. *Structure and physics of viruses: An integrated textbook*; Mateu, M. G., Ed.; Springer: New York, 2013.
(2) Christian, J. W. *The theory of transformations in metals and alloys: an advanced textbook in physical metallurgy*; Oxford: New York, 1981.
(3) Brown, A.; Clark, D.; Eastabrook, J.; Jepson, K. S. *Nature* **1964**, *201*, 914.
(4) Park, H. S.; Kwon, O.-H.; Baskin, J. S.; Barwick, B.; Zewail, A. H. *Nano Lett.* **2009**, *9*, 3954−3962.
(5) Kadau, K.; Germann, T. C.; Lomdahl, P. S.; Holian, B. L. *Science* **2002**, *296*, 1681−1684.
(6) Caspersen, K. J.; Carter, E. A. *Proc. Natl. Acad. Sci. U.S.A.* **2005**, *102*, 6738−6743.
(7) Turnbull, D. *J. Chem. Phys.* **1950**, *18*, 198−203.
(8) Miller, T. A.; Wittenberg, J. S.; Wen, H.; Connor, S.; Cui, Y.; Lindenberg, A. M. *Nat. Commun.* **2013**, *4*, 1369.
(9) Zheng, H.; Wang, J.; Huang, J. Y.; Wang, J.; Zhang, Z.; Mao, S. X. *Nano Lett.* **2013**, *13*, 6023−6027.
(10) Jacobs, K. *Science* **2001**, *293*, 1803−1806.
(11) Tolbert, S. H.; Alivisatos, A. P. *J. Chem. Phys.* **1995**, *102*, 4642−4656.
(12) Zheng, H.; Rivest, J. B.; MIller, T. A.; Sadtler, B.; Lindenberg, A. M.; Toney, M. F.; Wang, L. W.; Kisielowski, C.; Alivisatos, A. P. *Science* **2011**, *333*, 206−209.
(13) Morgan, B. J.; Madden, P. A. *Phys. Chem. Chem. Phys.* **2006**, *8*, 3304−3313.
(14) Grünwald, M.; Rabani, E.; Dellago, C. *Phys. Rev. Lett.* **2006**, *96*, 255701.
(15) Grünwald, M.; Dellago, C. *Nano Lett.* **2009**, *9*, 2099−2102.
(16) Mandal, T. *Appl. Phys. Lett.* **2012**, *101*, 021906.
(17) Reed, E. J. *Phys Rev B* **2010**, *81*, 144123.
(18) Wittenberg, J. S.; Merkle, M. G.; Alivisatos, A. P. *Phys. Rev. Lett.* **2009**, *103*, 125701.
(19) Armstrong, M. R.; Crowhurst, J. C.; Bastea, S.; Zaug, J. M. *J. Appl. Phys.* **2010**, *108*, 023511.
(20) Gahagan, K. T.; Moore, D. S.; Funk, D. J.; Rabie, R. L.; Buelow, S. J.; Nicholson, J. W. *Phys. Rev. Lett.* **2000**, *85*, 3205−3208.
(21) Dlott, D. D. *Annu. Rev. Phys. Chem.* **2011**, *62*, 575−597.
(22) Lee, I.-Y. S.; Hill, J. R.; Suzuki, H.; Dlott, D. D.; Baer, B. J.; Chronister, E. L. *J. Chem. Phys.* **1995**, *103*, 8313.
(23) Daranciang, D.; Highland, M.; Wen, H.; Young, S.; Brandt, N.; Hwang, H.; Vattilana, M.; Nicoul, M.; Quirin, F.; Goodfellow, J.; Qi, T.; Grinberg, I.; Fritz, D.; Cammarata, M.; Zhu, D.; Lemke, H.; Walko, D.; Dufresne, E.; Li, Y.; Larsson, J.; Reis, D.; Sokolowski-Tinten, K.; Nelson, K.; Rappe, A.; Fuoss, P.; Stephenson, G.; Lindenberg, A. *Phys. Rev. Lett.* **2012**, *108*, 087601.
(24) Emma, P.; Akre, R.; Arthur, J.; Bionta, R.; Bostedt, C.; Bozek, J.; Brachmann, A.; Bucksbaum, P.; Coffee, R.; Decker, F. J.; Ding, Y.; Dowell, D.; Edstrom, S.; Fisher, A.; Frisch, J.; Gilevich, S.; Hastings, J.; Hays, G.; Hering, P.; Huang, Z.; Iverson, R.; Loos, H.; Messerschmidt, M.; Miahnahri, A.; Moeller, S.; Nuhn, H. D.; Pile, G.; Ratner, D.; Rzepiela, J.; Schultz, D.; Smith, T.; Stefan, P.; Tompkins, H.; Turner, J.; Welch, J.; White, W.; Wu, J.; Yocky, G.; Galayda, J. *Nat. Photonics* **2010**, *4*, 641.
(25) Whitley, V. H.; McGrane, S. D.; Eakins, D. E.; Bolme, C. A.; Moore, D. S.; Bingert, J. F. *J. Appl. Phys.* **2011**, *109*, 013505.
(26) Suggit, M. J.; Higginbotham, A.; Hawreliak, J. A.; Mogni, G.; Kimminau, G.; Dunne, P.; Comley, A. J.; Park, N.; Remington, B. A.; Wark, J. S. *Nat. Commun.* **2012**, *3*, 1224.
(27) Milathianaki, D.; Boutet, S.; Williams, G. J.; Higginbotham, A.; Ratner, D.; Gleason, A. E.; Messerschmidt, M.; Seibert, M. M.; Swift, D. C.; Hering, P.; Robinson, J.; White, W. E.; Wark, J. S. *Science* **2013**, *342*, 220−223.
(28) Loveridge-Smith, A.; Allen, A.; Belak, J.; Boehly, T.; Hauer, A.; Holian, B.; Kalantar, D.; Kyrala, G.; Lee, R.; Lomdahl, P.; Meyers, M.; Paisley, D.; Pollaine, S.; Remington, B.; Swift, D.; Weber, S.; Wark, J. *Phys. Rev. Lett.* **2001**, *86*, 2349−2352.
(29) Rigg, P. A.; Gupta, Y. M. *Appl. Phys. Lett.* **1998**, *73*, 1655−1657.
(30) Bringa, E. M.; Rosolankova, K.; Rudd, R. E.; Remington, B. A.; Wark, J. S.; Duchaineau, M.; Kalantar, D. H.; Hawreliak, J.; Belak, J. *Nat. Mater.* **2006**, *5*, 805−809.
(31) Jacobs, K.; Wickham, J.; Alivisatos, A. P. *J. Phys. Chem B* **2002**, *106*, 3759−3762.
(32) Chen, C.; Herhold, A.; Johnson, C.; Alivisatos, A. *Science* **1997**, *276*, 398−401.
(33) *Landolt-Bornstein - Group III Condensed Matter*; Springer: New York, 1999; Vol. *41B*, pp 1−5.
(34) Zaziski, D.; Prilliman, S.; Scher, E. C.; Casula, M.; Wickham, J.; Clark, S. M.; Alivisatos, A. P. *Nano Lett.* **2004**, *4*, 943−946.